Supporting Information for

Atlantic Multidecadal Variability amplifies decadal variability in the Kuroshio–Oyashio Extension region under global warming

Yiting Wang[1,2], Shujun Li[1,3,4*], Lixin Wu[1,4], Chuan-Yang Wang[1,5*], Jingjie Yu[1,3]

[1]*Key Laboratory of Physical Oceanography/Frontier Science Centre for Deep Ocean Multispheres and Earth system, Ocean University of China; Qingdao, China.*

[2]*Academy of Future Ocean, Ocean University of China; Qingdao, China.*

[3]*Laboratory for Ocean Dynamics and Climate, Qingdao Marine Science and Technology Center; Qingdao, China.*

[4]*Laoshan Laboratory; Qingdao, China*

[5]*College of Oceanic and Atmospheric Sciences, Ocean University of China; Qingdao, China.*

*Corresponding author:

Shujun Li (lishujun@ouc.edu.cn) and Chuan-Yang Wang (wangchuanyang@ouc.edu.cn)

Contents:

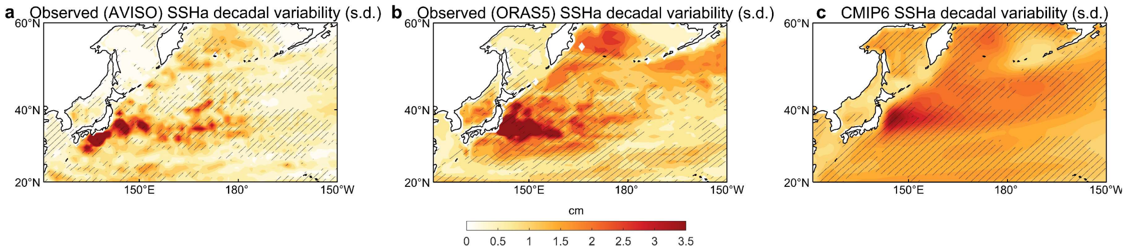

Supplementary Fig. 1 | Observed and simulated decadal variability of sea surface height anomalies (SSHa) over the North Pacific. a Decadal variability intensity of SSHa, quantified as the standard deviation at each grid point (shading; unit: cm). The SSHa time series is quardratically detrended and smoothed with an 11-year running, based on the AVISO for 1993–2022. **b** same as (**a**), but for the ORAS5 for 1958–2025. **c** Same as (**a**), but for the multi-model ensemble mean (MMEM) results in historical simulations from CMIP6. All analyses are first performed for each individual model, and the MMEM is then calculated as the equally weighted arithmetic mean across models. The statistical significance of decadal variability is assessed at each grid point using power spectral analysis based on a red noise null hypothesis, with hatched regions indicating decadal signals statistically significant at the 95% confidence level.

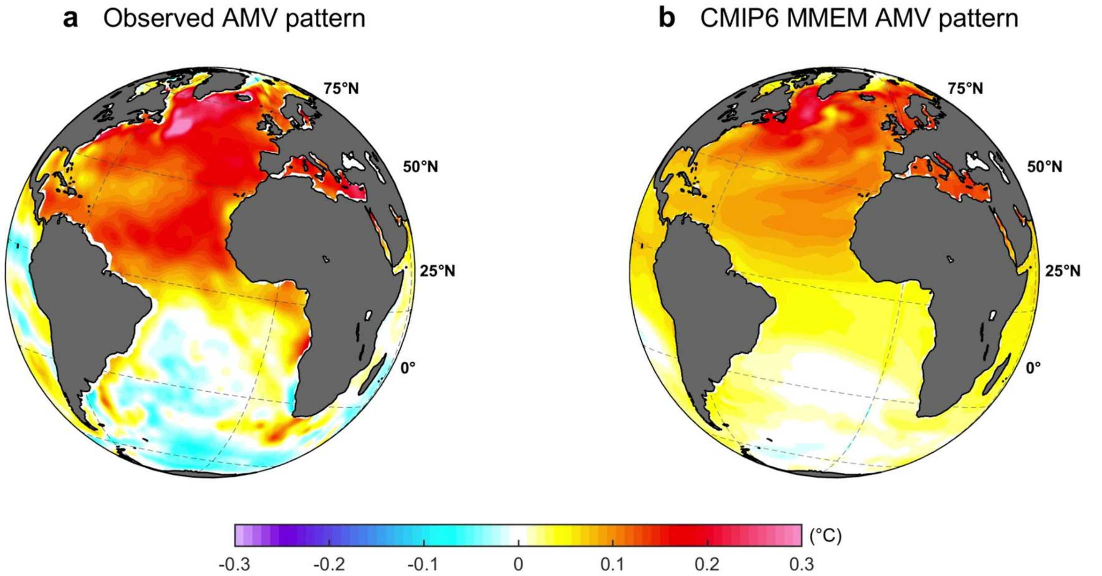

Supplementary Fig. 2 | CMIP6 models capture the key characteristics of observed Atlantic Multidecadal Variability (AMV). **a** Regression of quadratically detrended and 11-yr running mean sea surface temperature anomalies (shading; unit: °C) onto the normalized AMV index, based on the HadISST1. **b** same as (**a**), but for the historical simulations in CMIP6. Shown is the multi-model ensemble mean result.

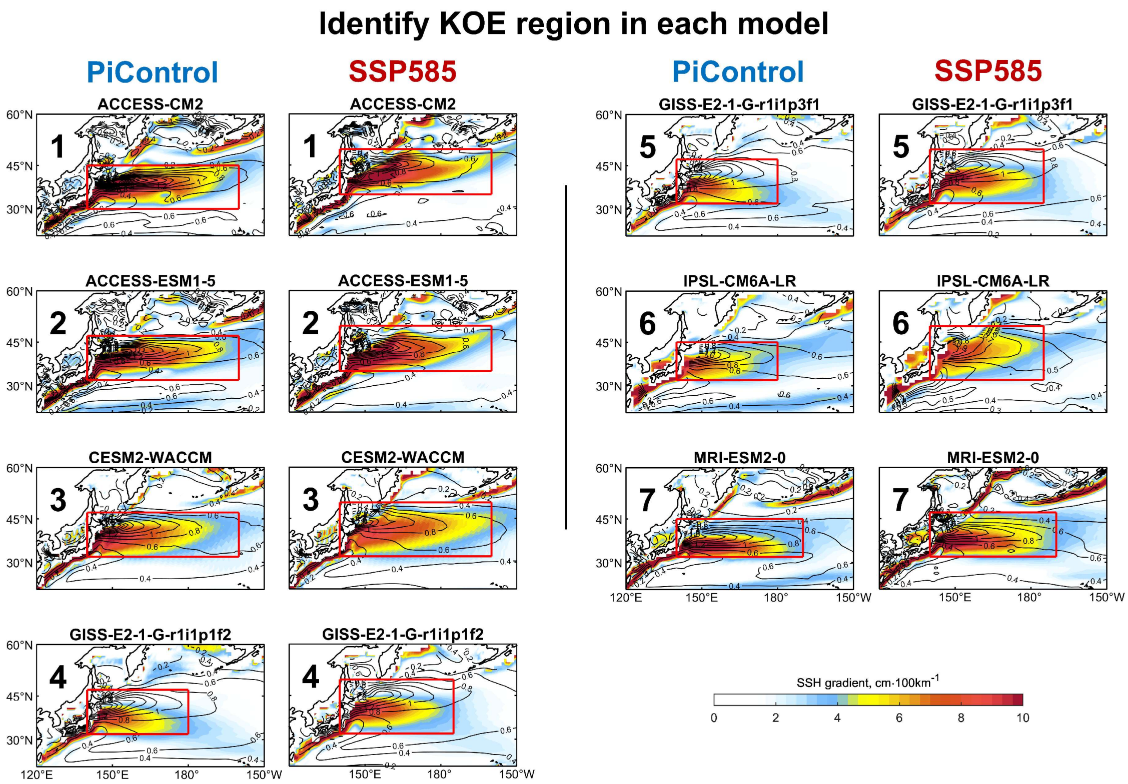

Supplementary Fig. 3 | Climatology of meridional SSH and SST gradients in the Kuroshio–Oyashio Extension (KOE) region across individual CMIP6 models under PiControl and SSP585. Mean meridional SSH gradients (shading; unit: cm·100 km^{-1}) and SST gradients (contours; unit: °C·100 km^{-1}) are shown for seven CMIP6 models (model identifiers are indicated in the upper-left corner of each panel). The red box highlights the KOE region in each model.

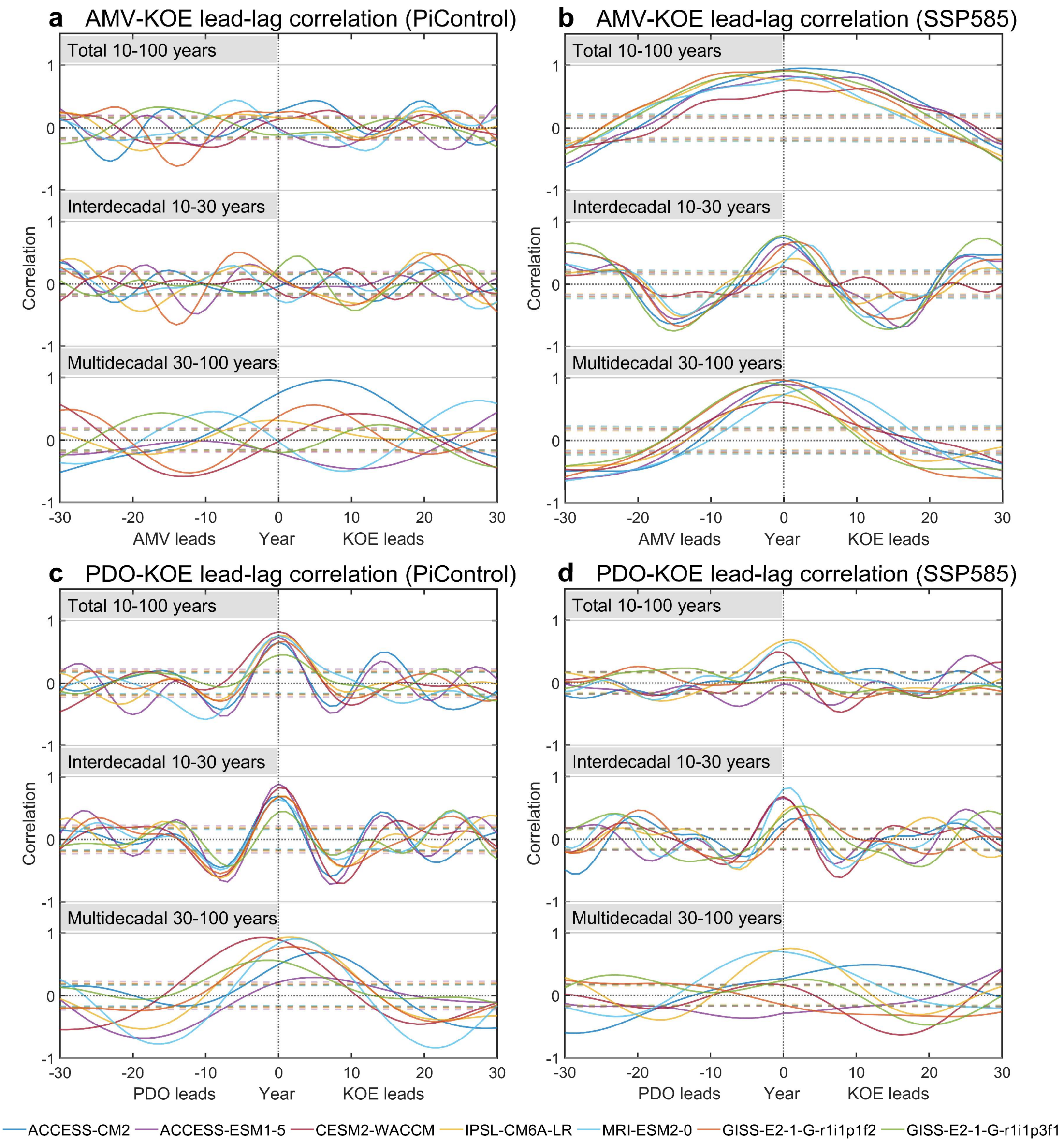

Supplementary Fig. 4 | Lead–lag correlations of AMV–KOE and PDO–KOE across different frequency bands in each model and simulation. (**a, b**) Lead–lag correlation between AMV index and KOE SSH index under PiControl (**a**) and SSP585 (**b**) simulations. (**c, d**) Lead–lag correlation between PDO index and KOE SSH index under PiControl (**c**) and SSP585 (**d**) simulations. Colored solid lines represent individual models. Horizontal dashed lines indicate significance thresholds for each model at the 95% confidence level. In each panel, the first row shows correlations for the 10–100 years band-pass filtered AMV, PDO, and KOE indices, the second row shows correlations based on the interdecadal (10–30-year) band-pass filtered indices, and the third row shows correlations based on the multidecadal (30–100-year) band-pass filtered indices.

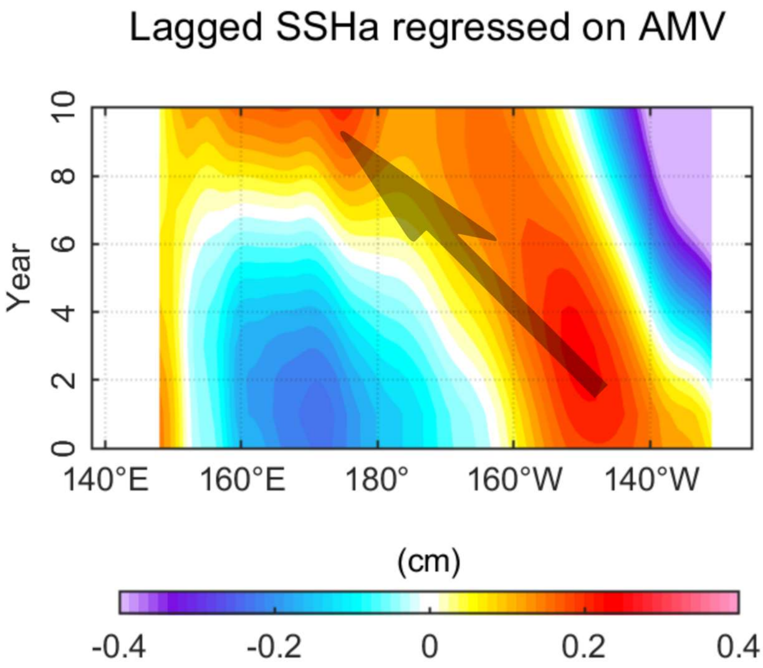

Supplementary Fig. 5 | Evolution of westward-propagating sea surface height anomalies (SSHa) over North Pacific midlatitudes associated with Atlantic Multidecadal Variability (AMV). Hovmöller diagram of SSHa (averaged over 35°–50°N; unit: cm) regression onto the normalized AMV index under SSP585 scenario. The y-axis denotes the lag years of SSHa relative to the AMV index.

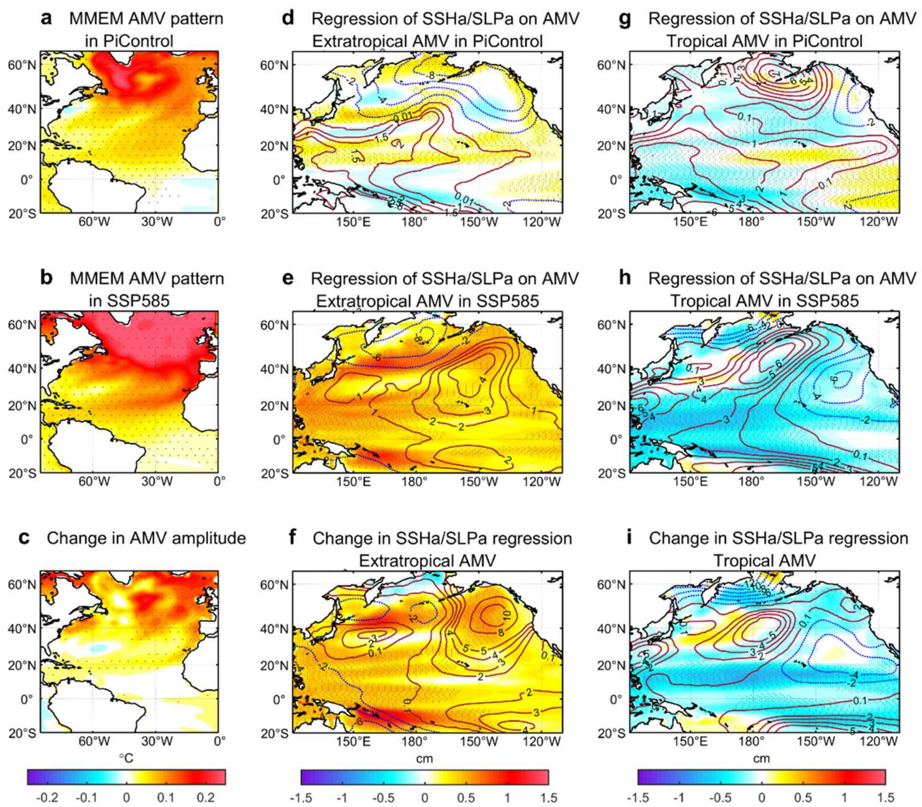

Supplementary Fig. 6 | Projected increase in the amplitude of the Atlantic Multidecadal Variability (AMV) and the teleconnection from the tropical and extratropical components of AMV to North Pacific under global warming in CMIP6. a The AMV pattern in PiControl, derived from the regression of sea surface temperature anomalies (SSTa) onto the normalized AMV index. Shown is the multi-model ensemble mean (MMEM) result, which is constructed by averaging these model-specific AMV-related patterns. Grey dots indicate regions with statistically significant inter-model consistency at the 80% confidence level from a bootstrap test. **b** Same as **a**, but for the SSP585 scenario. **c** Changes in the AMV pattern (shading; unit: °C) under global warming (SSP585 minus PiControl). Grey lines denote the changes are significant at the 95% confidence level in a bootstrap test. Shown is the MMEM result. **d** Regressions of sea surface height anomalies (SSHa, shading; unit: cm) and surface level pressure anomalies (SLPa, contours; unit: Pa) onto the normalized extratropical AMV index in PiControl. The AMV index here is defined as the area-weighted average of sea SSTa over the midlatitudes (75°W–7°W, 20°N–70°N) to isolate the extratropical component. Shown is the MMEM result. Grey dots indicate regions with statistically significant inter-model consistency at the 80% confidence level from a bootstrap test. **e** Same as (**d**), but in SSP585 scenario. **f** Differences between (**d**) and (**e**) (SSP585 minus PiControl). Grey dots denote regions where SSHa changes are significant at the 95% confidence level based on a bootstrap test. **g, h, i** Same as (**d**), (**e**), (**f**), respectively, but for the tropical AMV index, defined as the area-weighted average of SSTa over the tropics (75°W–15°E, 20°S–20°N). All shown regression coefficients are obtained by controlling for the extratropical AMV, tropical AMV, and PDO indices within a multiple linear regression framework.

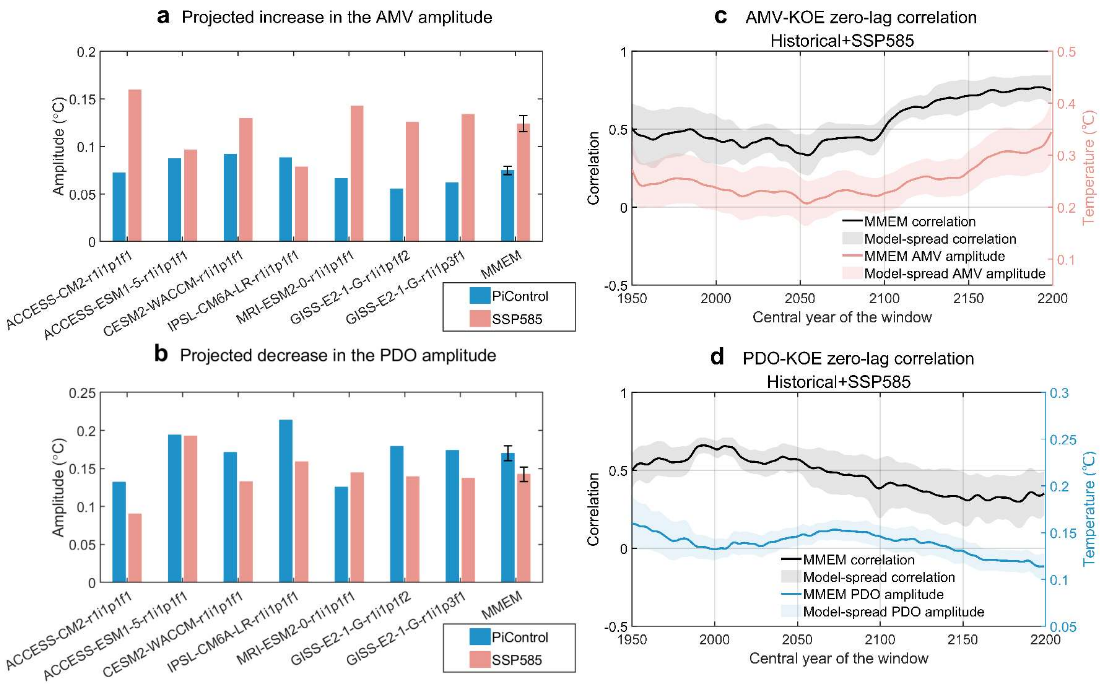

Supplementary Fig. 7 | The projected changes in the Atlantic Multidecadal Variability (AMV) and Pacific Decadal Oscillation (PDO) amplitude and their running correlations with KOE variability under global warming. a Comparison of the AMV amplitude between PiControl (blue bars) and SSP585 (red bars) simulations. Error bars on the multi-model ensemble mean (MMEM) correspond to ±1 standard deviation of 10000 inter-realizations of a bootstrap method. **b** same as (**a**), but for PDO amplitude. **c** Running zero-lag correlation coefficients between the AMV and KOE indices. Correlations are calculated using a 101-year sliding window in the historical and SSP585 simulations. The black solid line denotes the MMEM of correlations based on the seven CMIP6 models (left y-axis), and the shaded envelopes represent ±0.5 standard deviations across the models. The red line shows the MMEM of the AMV amplitude (°C, right axis), and the red shading indicates ±0.5 standard deviations across the models. The years shown on the x-axis correspond to the central year of each 101-year sliding window. **d** Same as in (**c**), but for the PDO and KOE indices. The blue line shows the MMEM of the PDO amplitude (°C, right y-axis), and the blue shading indicates ±0.5 standard deviations across the models.

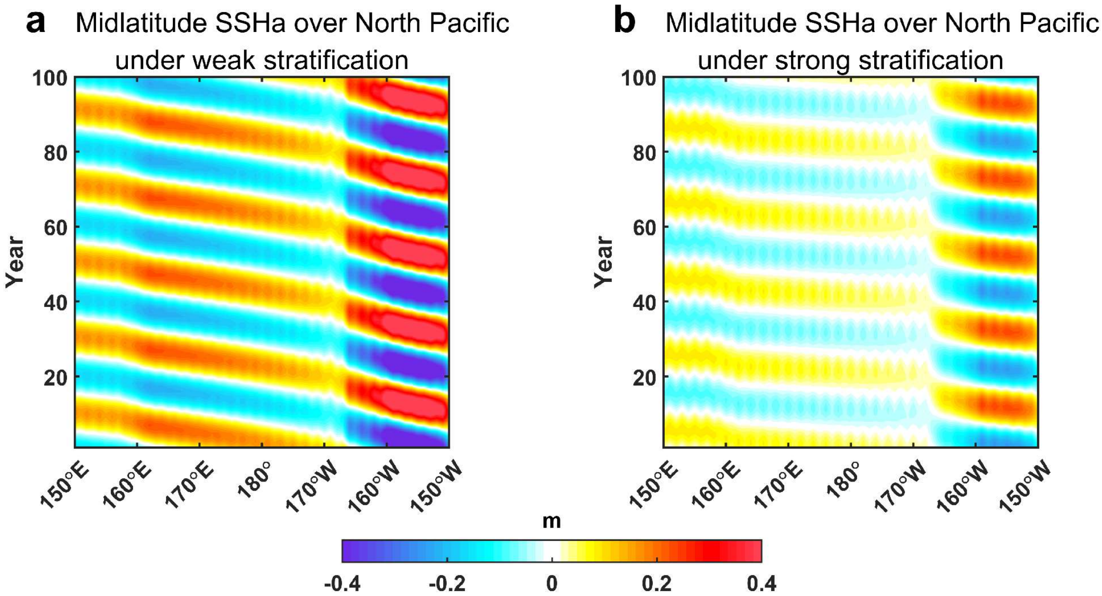

Supplementary Fig. 8 | The modulation of ocean stratification on decadal sea surface height (SSH) variability over the North Pacific. a Longitude-time hovmöller diagram of the midlatitude (averaged over 35°N–50°N) SSHa (shading; unit: m) over North Pacific under weak stratification based on the 1.5-layer reduced gravity ocean model. **b** same as (**a**), but under strong stratification.

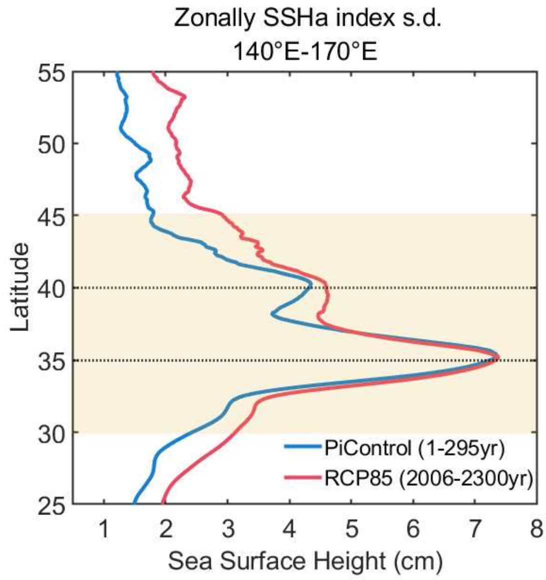

Supplementary Fig. 9 | Projected changes in the zonally averaged sea surface height anomalies (SSHa) under global warming simulated by CESM-HR. Comparison of the intensity and peak latitude of the zonally averaged (140°E–170°E) SSHa in KOE region between PiControl (blue) and RCP85 (red) in CESM-HR simulations. The intensity is measured by the standard deviation of SSHa.

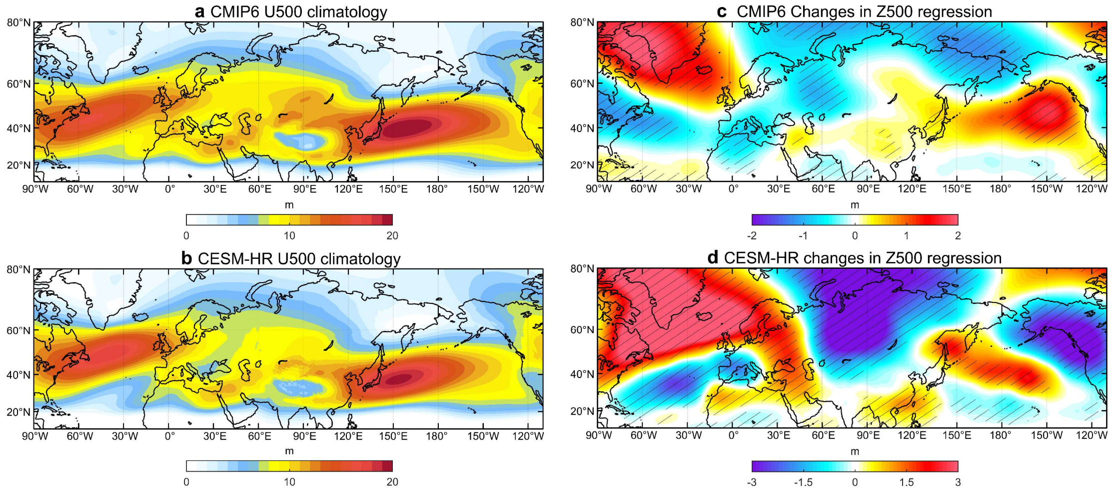

Supplementary Fig. 10 | Climatological zonal mean flow and AMV-related 500 hPa geopotential height (Z500) anomalies in CMIP6 models and CESM-HR. a, Climatological zonal wind at 500 hPa (U500) under SSP585, averaged across CMIP6 models. **b**, Same as **a**, but for the CESM-HR under RCP85. **c**, Regression of Z500 anomalies onto the AMV index, showing the difference between SSP585 and PiControl in CMIP6 models. Hatched areas indicate regions where changes under global warming are significant at the 95% confidence level. **d**, Same as **c**, but for the CESM-HR.

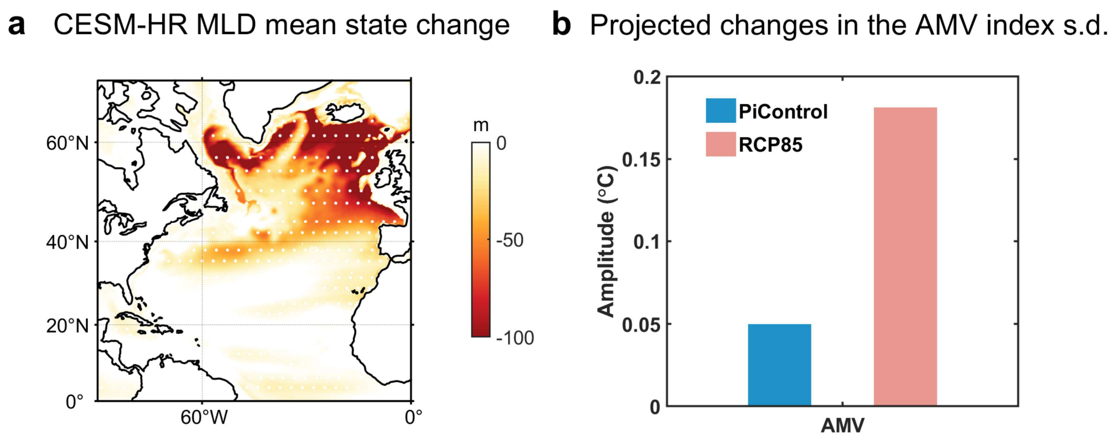

Supplementary Fig. 11 | Projected changes in the climatological mixed layer depth (MLD) and amplitude of Atlantic Multidecadal Variability (AMV) under global warming simulated by CESM-HR. a Changes in the climatological MLD under global warming over the North Atlantic (RCP85 minus PiControl; shading; unit: m). The white dots indicate where the differences are significant at the 95% confidence level in a bootstrap test. **b** Comparison of the standard deviation (unit: °C) of the AMV index between the PiControl (blue bars) and RCP85 scenarios (red bars).

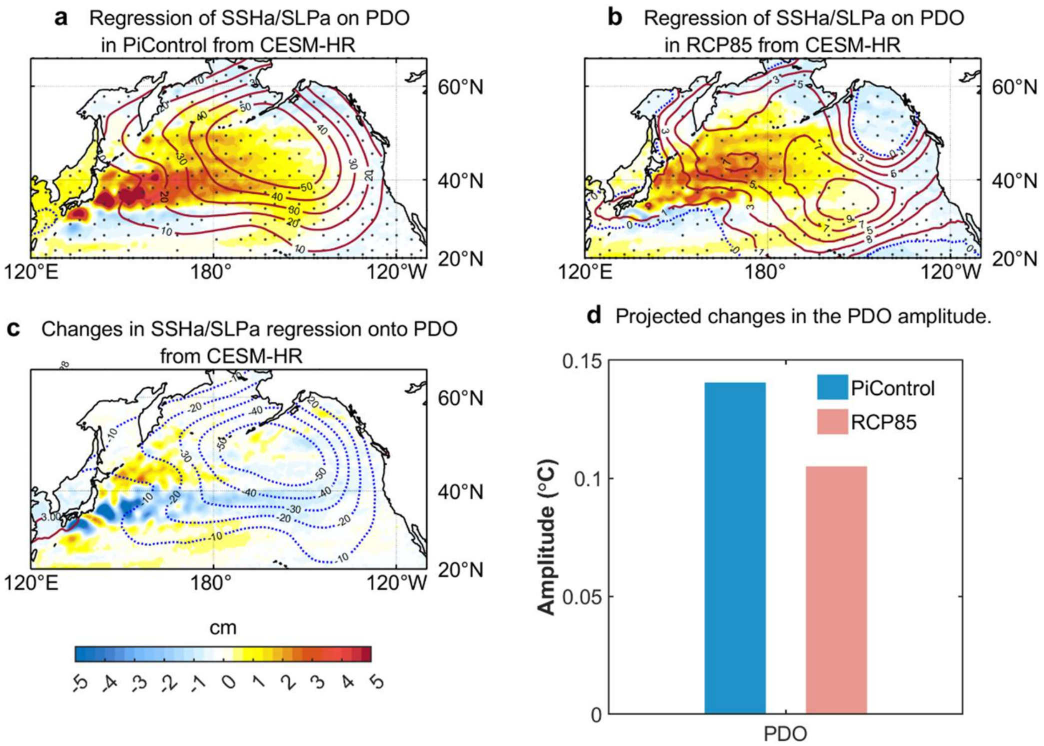

Supplementary Fig. 12 | The reduced role of Pacific Decadal Oscillation (PDO) in modulating decadal variability in the Kuroshio–Oyashio Extension (KOE) region under global warming in CESM-HR. a Regressions of 11-yr running-mean and detrended SSHa (shading; unit: cm) and surface level pressure anomalies (SLPa, contours with positive in red and negative in blue; unit: Pa) onto the normalized PDO index. Shown are PDO-related regression patterns derived from a multiple linear regression conditional on the Atlantic Multidecadal Variability. The grey dots indicate regions where the coefficient is statistically significant at the 95% level based on a *t*-test. **b** Same as (**a**), but for the RCP85 scenario; **c** Differences between the regressions of (**a**) and (**b**) (RCP85 minus PiControl). **d** Comparison of the PDO amplitude (unit, °C) between the PiControl (blue bars) and RCP85 scenarios (red bars).

Supplementary Tab. 1 | The CMIP6 models and experiments used in this study.

Institute, Country	Model	Variant Label	Experiments					
			PiControl	Historical	SSP1-2.6	SSP2-4.5	SSP3-7.0	SSP5-8.5
Commonwealth Scientific and Industrial Research Organization and Bureau of Meteorology (CSIRO-BOM), Australia	ACCESS-CM2	r1i1p1f1	√	√	√			√
	ACCESS-ESM1-5	r1i1p1f1	√	√	√			√
National Science Foundation, Department of Energy, National Center for Atmospheric Research (NSF-DOE-NCAR), United States	CESM2-WACCM	r1i1p1f1	√	√	√			√
Goddard Institute for Space Studies (GISS), United States	GISS-E2-1-G	r1i1p1f2	√	√	√	√	√	√
		r1i1p3f1	√	√	√	√		√
	GISS-E2-2-G	r1i1p3f1	√	√	√	√		
Institute Pierre-Simon Laplace (IPSL), France	IPSL-CM6A-LR	r1i1p1f1	√	√	√			√
Meteorological Research Institute (MRI), Japan	MRI-ESM2-0	r1i1p1f1	√	√	√			√